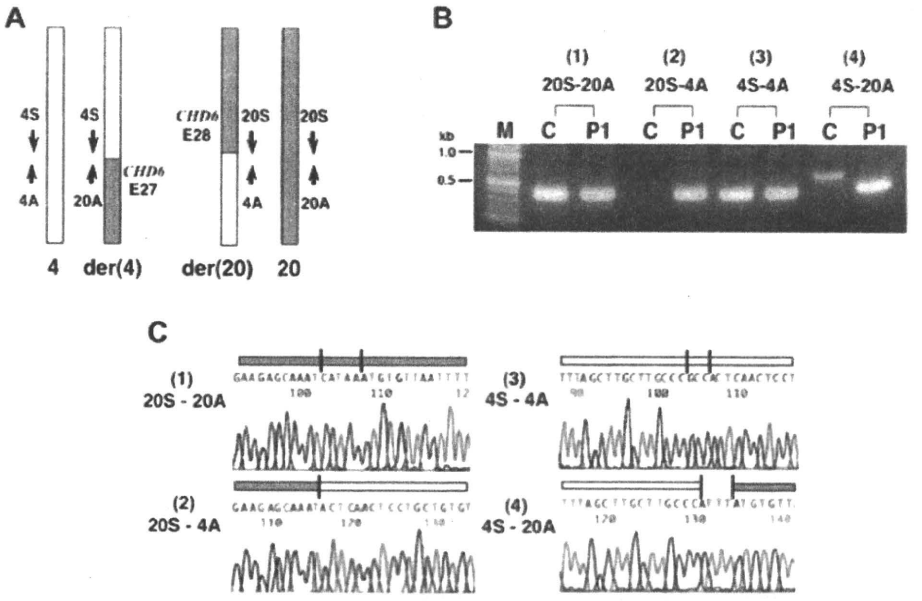

FIG. 4. Nucleotide sequences of the breakpoints. A: Schematic representation of normal and derivative chromosomes 4 and 20 of patient 1. Primer pairs 4S-20A and 20S-4A were designed for amplification of DNA fragments including breakpoints on der(4) and der(20), respectively. Primer pairs 4S-4A and 20S-20A amplified DNA fragments containing the sequences around the breakpoints on chromosomes 4 and 20, respectively. The open box represents all and part of chromosome 4. The closed box represents all and part of chromosome 20. der(4) contains exons 1–27 of *CHD6* and der(20) contains exons 28–37 of *CHD6*. B: PCR amplification of DNA fragments from normal and derivative chromosomes with specific primer pairs. C, control; P1, patient 1; M, 100 bp DNA ladder. C: Sequence chromatograms of the DNA fragments amplified with the specific primer pairs (1) 20S-20A, (2) 20S-4A, (3) 4S-4A, and (4) 4S-20A.

which showed a linear correlation of products with the number of cycles performed [Wakamatsu et al., 1992]. This analysis showed the steady-state level of the patient's *CHD6* mRNA to be decreased to ~50% of those of three normal controls while the steady-state levels of *SH3RF1* and *NEK1* mRNA were as same as in controls (Fig. 5A). We next confirmed decreased expression of the patient's *CHD6* mRNA by Northern blot analysis using a part of the 5′- or 3′-region of *CHD6* cDNA as a probe. Steady-state levels of the patient's *CHD6* mRNA was decreased to ~50% but of similar size (~10 kb) to those of controls (Fig. 5B). No other size of *CHD6* mRNA was detected in the patient's lymphoblastoid cells (Fig. 5B).

Tissue Distribution and Developmental Expression of CHD6 and Its Mouse Ortholog

Northern blot analysis using a *CHD6* probe (exons 34–37, 1,221 bp) on mRNA samples from 12 different tissues of human adults revealed expression of a 10.4-kb mRNA in brain, heart, skeletal muscle, kidney, small intestine, placenta, lung, and peripheral blood leukocytes (Fig. 5C). Expression was most pronounced in skeletal muscle and barely detectable in colon, thymus, spleen, and liver. In mouse cerebral cortex, orthologous *Chd6* mRNA expression was detected at E15.5 and increased gradually after birth (P0-28) (Fig. 5D).

Knockdown of CHD6 or CHD7 Results in Impairment of Chromosome Alignment

As CHD proteins are nucleosome-remodeling factors, we hypothesized that cells from patients with loss of function mutations in CHD subfamily III genes (i.e., *CHD6* and *CHD7*) may have defects in chromosome dynamics during the cell cycle. To study this hypothesis, we knocked down CHD6 or CHD7 expression in HeLa cells by transfection of siRNA expression vectors (Fig. 6A), and analyzed chromosome dynamics of metaphase cells. The frequency misaligned chromosomes on the metaphase plate ("plentiful" in Table I) was increased by at least twofold in CHD6 or CHD7 knockdown HeLa cells than in control cells (no treatment or pSUPER transfection) (Table I and Fig. 6B).

Patients With CHD6 or CHD7 Mutations Exhibit Aneuploidy

Chromosomal preparations were made from lymphoblastoid cells using standard method. Analysis of 300 metaphase lymphoblastoid cells from patients 1–3 and three normal controls revealed that all patients have a rate of abnormal chromosome number of >15.6%. This frequency of aneuploidy is more than twice the abnormal chromosome rate in control cells (<7.7%, Table II).

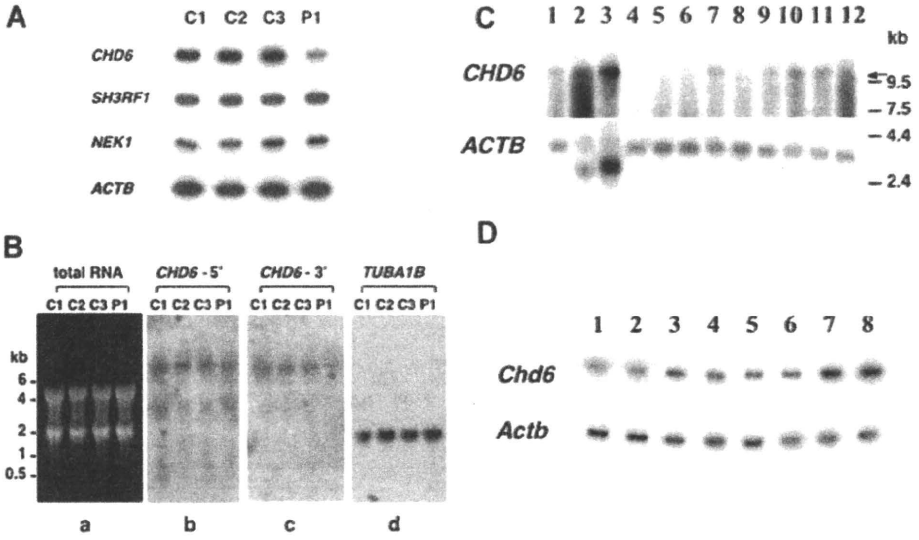

FIG. 5. CHD6 expression profiles. A: RT-PCR analysis of *CHD6*, *SH3RF1*, and *NEK1* mRNA in patient 1 and normal lymphoblastoid cells using RT-PCR. The amount of *ACTB* mRNA was used as a standard to estimate the amounts of other mRNAs. PCR cycles for each gene were as follows: *CHD6*, 22; *SH3RF1*, 24; *NEK1*, 26; *ACTB*, 16. C1-3, normal controls; P1, patient 1. B: Northern blot analyses of lymphoblastoid cells from three normal controls and patient 1. Total RNAs (10 μg) of lymphoblastoid cells from three controls and patient 1 were separated on a 0.9% formaldehyde/agarose gel, stained using ethidium bromide (a), transferred to Hybond N+ membrane, and hybridized using an [α-^{32}P]-labeled 5′-*CHD6* probe (b). After removal of the probe, the same membrane was hybridized with [α-^{32}P]-labeled 3′-*CHD6* probes (c), and *TUBA1B* (d). C1-3, normal controls; P1, patient 1. C: Expression patterns of *CHD6*. Autoradiographs of Northern blots hybridized with a 1.2-kb *CHD6* cDNA (exons 34–37) and a 2.0-kb human *ACTB* (β-actin) cDNA as a standard. Lane 1, brain; lane 2, heart; lane 3, skeletal muscle; lane 4, colon; lane 5, thymus; lane 6, spleen; lane 7, kidney; lane 8, liver; lane 9, small intestine; lane 10, placenta; lane 11, lung; and lane 12, peripheral blood leukocyte. *CHD6* mRNA was ~10.4 kb in size, and is indicated by an arrow. D: Expression patterns of *Chd6* in mouse cerebral cortex. Total RNA was extracted from mouse cerebral cortex at various ages and steady-state levels of *Chd6* mRNA and *Actb* mRNA were analyzed by RT-PCR. Lane 1, E15.5; lane 2, P0; lane 3, P1; lane 4, P2; lane 5, P4; lane 6, P7; lane 7, P14; lane 8, P28.

DISCUSSION

In this study, we report a patient (patient 1) with a balanced translocation t(4;20)(q33;q12) presenting with severe mental retardation, brachydactyly of the toes and minor anomalies of the face. We localized the translocation breakpoint to intron 27 of *CHD6*, and Northern blot analysis using 5′- and 3′-probes showed the steady-state levels of *CHD6* mRNA in lymphoblastoid cells of the patient to be decreased by ~50% without any alteration in transcript size. Thus, haploinsufficiency of *CHD6* is most likely responsible for the clinical features of patient 1. We searched reported cases of patients harboring aberrant chromosome structures (deletions or translocations) around *CHD6* locus (20q12). Recently, a female harboring a de novo translocation t(18;20)(q21.1;q11.2) with moderate mental retardation and minor facial anomalies was reported [Kalscheuer et al., 2008]. In this case, the breakpoint of 18q21.1 was located in intron 3 of *TCF4*, whereas the breakpoint of 20q11.2 was located in intron 1 (exon 1 contains only the 5′-untranslated region) of *CHD6*. Moreover, fusion transcripts of the genes were identified. Thus, this is not a case of *CHD6* haploinsufficiency. A female with interstitial microdeletion of 20q11.22-q12 has also been reported, but *CHD6* was not included in the deletion area [Callier et al., 2006]. Taken together, patient 1 is the first reported case of symptoms resulting from *CHD6* haploinsufficiency. Identification and characterization of similar cases with breakpoints, deletions, or mutations involving *CHD6* is necessary to clarify the clinical features of *CHD6* haploinsufficiency.

CHD6 belongs to the largest subfamily, subfamily III (CHD6–9), of the CHD family of proteins (CHD1–9), which were recently found to possess ATP-dependent chromosome-remodeling activity and an ability to regulate transcription through mobilization of chromatin structures [Nioi et al., 2005; Shur et al., 2006; Yuan et al., 2007; Thompson et al., 2008]. These functions are associated with chromo-domains and an SNF2-related helicase/ATPase domain, both common to all CHD family proteins (CHD1–9). CHD6–9 are very large proteins (>300 kDa) containing other domains on the N-terminal and C-terminal sides of these common domains. Moreover, CHD6 and CHD7 have very similar amino acid sequence and the C-terminal 610 amino acids of CHD6 show 35% homology with the C-terminal 670 amino acids of CHD7. To investigate the cellular mechanism of disease in patient 1 resulting from CHD6 haploinsufficiency, we reduced CHD6 or CHD7 function by RNA interference in HeLa cells and examined chromosome dynamics during the cell cycle. Our studies demonstrated that the frequencies of cells with extensively misaligned chromosomes ("plentiful" in Table I) were increased at least twofold upon CHD6- or CHD7-knockdown. During mitosis, duplicated sister chromatids condense gradually, align to the metaphase plate, and subsequently segregate to oppos-

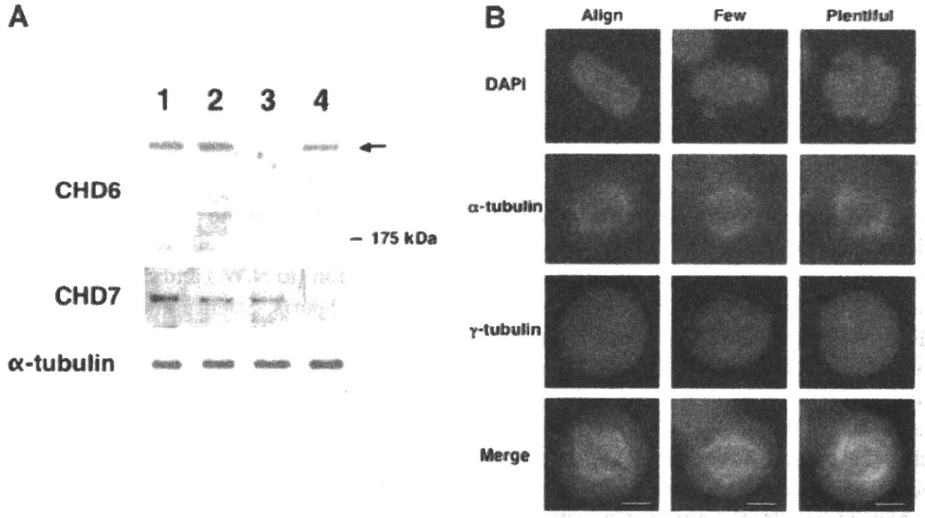

FIG. 6. Effects of RNAi-mediated knockdown of CHD6 or CHD7 on chromosome alignment in metaphase HeLa cells. A: RNAi-mediated knockdown of CHD6 or CHD7. pSUPER-siCHD6, pSUPER-siCHD7, or pSUPER (control vector) were transfected into HeLa cells. At 60 hr after transfection, cells were harvested and proteins were extracted and analyzed by Western blot analyses using antibodies specific for α-tubulin, CHD6 and CHD7. Lane 1, non-trasfected HeLa cells; lane2, pSUPER; lane 3, pSUPER-siCHD6; lane 4, pSUPER-siCHD7. The arrow indicates signals for CHD6, and the protein-molecular marker (175 kDa) is shown on the panel of CHD6. B: Misaligned chromosomes in CHD6- or CHD7-knockdown HeLa cells. pSUPER-siCHD6, pSUPER-siCHD7, or pSUPER were transfected into HeLa cells. At 60 hr after transfection, cells were fixed and stained with anti-α-tubulin (red) and anti-γ-tubulin antibodies (green). Chromosomes were stained with DAPI (blue). Images represent cells containing aligned chromosomes (aligned, left), one or two misaligned chromosomes (few, middle), and three or more misaligned chromosomes (plentiful, right), respectively. Scale bar indicates 10 μm.

TABLE I. Effects of RNAi-Mediated Knockdown of CHD6 or CHD7 on Chromosome Alignment in Metaphase HeLa Cells

Alignment	Control % (n)	Vector (pSUPER) % (n)	CHD6 (pSUPER) % (n)	CHD7 (pSUPER) % (n)	siRNA (control) % (n)	siRNA (CHD6) % (n)
Aligned	88.0 (938)	86.6 (428)	76.1 (290)	77.5 (238)	87.0 (559)	76.8 (464)
Few	5.4 (57)	5.7 (28)	6.8 (26)	4.9 (15)	6.2 (40)	7.1 (43)
Plentiful	6.6 (70)	7.7 (38)	**17.1** (65)	**17.6** (54)	6.8 (44)	**16.1** (97)
Total	100 (1,065)	100 (494)	100 (381)	100 (307)	100 (643)	100 (604)

Bold typing means the significance of group differences (p-value of <0.05) analyzed with one-way analysis of variance followed by Bonferroni correction for multiple comparisons.

ing spindle poles. Precise alignment of the chromosomes at the metaphase plate is crucially important because misaligned chromosomes may cause mitotic arrest and/or premature segregation which can lead to aneuploidy and/or cell death. Toyoda and Yanagida [2006] reported that cells displaying extensively misaligned chromosomes are remarkably increased in HeLa cells knocked down for hRad21, a component of the cohesin complex. The authors concluded that this is the earliest phenotype in cells harboring mitotic delay. Thus, the increase in the amount of extensively misaligned chromosomes in CHD6- or CHD7-knock-

TABLE II. Chromosome Numbers of Lymphoblastoid Cells From Patients 1–3 and Normal Controls

2n	41	42	43	44	45	46	47	48	49	50	51	52	53	54	55	56	57	Aneuploidy (%)
Control 1	1		1	4	15	277	1	1										7.7
Control 2				4	10	283	2	1										5.7
Control 3			1	8	11	278	1		1									7.3
P1 (CHD6)		5	6	14	19	245	7	1		1	1					1		18.3
P2 (CHD7)	1	2	5	9	20	251	7	2	1				1				1	16.3
P3 (CHD7)			3	9	24	253	10	1										15.6

down HeLa cells suggests that these two proteins also play important roles in chromosome alignment at metaphase.

A recent study demonstrated that other CHD family proteins, specifically subfamily II members (CHD3 and CHD4), also play important roles in chromosome dynamics. CHD3 predominantly co-localized with pericentrin (a component of pericentriolar materials, an electron-dense matrix which surrounds the centrosome) at metaphase and CHD3-knockdown HeLa cells exhibited dissociation of pericentrin from centrosomes, which caused metaphase delay, mitotic failure, and cytokinesis defects. Additionally, CHD4 negatively regulates the amount of pericentrin at the centrosome [Sillibourne et al., 2007]. Thus, CHD subfamily II and III proteins are associated with chromosome alignment at metaphase. Since CHD6 and CHD7 are diffusely localized throughout the cell at metaphase (supporting information Fig. 1, supporting information Fig. 1 may be found in the online version of this article), the cellular mechanism resulting in misaligned chromosomes in CHD6- or CHD7-knockdown cells likely differs from the mechanism in CHD3-knockdown cells. Further study is required to clarify the role of CHD6 and CHD7 in chromosome alignment in more detail.

It is important to analyze chromosome alignment in patients' cells to evaluating the pathogenesis of disease. We used lymphoblastoid cells for this purpose. Because lymphoblastoid cells are suspension cells, it is difficult to analyze chromosome alignment directly. Instead, we examined aneuploidy (an incorrect number of chromosomes) of the lymphoblastoid cells. The observed elevated frequency of aneuploidy is suggestive that the patients have abnormal chromosome alignment as a result of CHD6 or CHD7 mutation. In humans, aneuploidy is the major cause of miscarriages and mental retardation [Pai et al., 2003]. A relatively minor two- to threefold increase of aneuploidy might account, at least in part, for mental retardation of patients 1–3, which is more mild than cancer or prenatal death.

CHD7 is the only gene known to be causal for CHARGE syndrome. Curiously, the clinical features of patient 1 are quite different from those of the established CHARGE syndrome caused by *CHD7* mutation, save for mental retardation. Using chromatin immunoprecipitation on tiled microarrays (ChIP-chip), CHD7 was localized to discrete locations along chromatin specific to each cell type and ES cell differentiation state [Schnetz et al., 2009]. Thus, differences in target genes regulated by the chromatin-remodeling activity of CHD6 or CHD7 may explain the range of clinical features.

Kulkarni et al. [2008] reported a female patient with a de novo translocation in *CHD2* presenting scoliosis, hirsutism, learning problems, and developmental delay, syndactyly of the toes should also be noted. Brachydactyly is defined as disproportionately short fingers and toes, and forms part of the group of limb malformations [Temtamy and McKusick, 1978]. Our patient showed brachydactyly of the middle phalanx of toes. Nearly two-thirds (19/31) of individuals suffering from CHARGE syndrome have scoliosis [Doyle and Blake 2005]. Moreover, CHD9 regulates transcription during differentiation of osteogenic cells [Shur and Benayahu, 2005; Shur et al., 2006]. Thus, mutations of CHD family genes are candidate causal factors in patients with abnormal development of bones.

In summary, we have reported the first patient with a mutation identified in *CHD6* which is causative for mental retardation with minor anomalies. We also showed that loss of function mutations of *CHD6* or *CHD7* are associated with impairment of chromatin/chromosome assembly during mitosis.

ACKNOWLEDGMENTS

We are grateful to the patients who participated in this study and their families. This study was supported by the Uehara Memorial Foundation (to N.W.) and grants from the Ministry of Education, Culture, Sports, Science and Technology of Japan (to K.Y. and N.W.).

REFERENCES

Callier P, Faivre L, Marle N, Thauvin-Robinet C, Sanlaville D, Gosset P, Pieur M, Labenne M, Huet F, Mugneret F. 2006. Major feeding difficulties in the first reported case of interstitial 20q11.22-q12 microdeletion and molecular cytogenetic characterization. Am J Med Genet Part A 140A:1859–1863.

Doyle C, Blake K. 2005. Scoliosis in CHARGE: A prospective survey and two case reports. Am J Med Genet Part A 133A:340–343.

Ishihara K, Oshimura M, Nakao M. 2006. CTCF-dependent chromatin insulator is linked to epigenetic remodeling. Mol Cell 23:733–742.

Kalscheuer VM, Feenstra I, Van Ravenswaaij-Arts CM, Smeets DF, Menzel C, Ullmann R, Musante L, Ropers HH. 2008. Disruption of the TCF4 gene in a girl with mental retardation but without the classical Pitt-Hopkins syndrome. Am J Med Genet Part A 146A:2053–2059.

Kulkarni S, Nagarajan P, Wall J, Donovan DJ, Donell RL, Ligon AH, Venkatachalam S, Quade BJ. 2008. Disruption of chromodomain helicase DNA binding protein 2 (CHD2) causes scoliosis. Am J Med Genet Part A 146A:1117–1127.

Lutz T, Stoger R, Nieto A. 2006. CHD6 is a DNA-dependent ATPase and localizes at nuclear sites of mRNA synthesis. FEBS Lett 580: 5851–5857.

Nioi P, Nguyen T, Sherratt PJ, Pickett CB. 2005. The carboxy-terminal Neh3 domain of Nrf2 is required for transcriptional activation. Mol Cell Biol 25:10895–10906.

Pai GS, Lewandowski RC, Borgaonkar DS. 2003. Handbook of chromosomal syndromes. New York: Wiley-Liss.

Pinkel D, Landegent J, Collins C, Fuscoe J, Segraves R, Lucas J, Gray J. 1988. Fluorescence in situ hybridization with human chromosome-specific libraries: Detection of trisomy 21 and translocations of chromosome 4. Proc Natl Acad Sci USA 85:9138–9142.

Schnetz MP, Bartels CF, Shastri K, Balasubramanian D, Zentner GE, Balaji R, Zhang X, Song L, Wang Z, LaFramboise T, Crawford GE, Scacheri PC. 2009. Genomic distribution of CHD7 on chromatin tracks H3K4 methylation patterns. Genome Res 19:590–601.

Schuster EF, Stoger R. 2002. CHD5 defines a new subfamily of chromodomain-SWI2/SNF2-like helicases. Mamm Genome 2:117–119.

Shur I, Benayahu D. 2005. Characterization and functional analysis of CReMM, a novel chromodomain helicase DNA-binding protein. J Mol Biol 352:646–655.

Shur I, Socher R, Benayahu D. 2006. In vivo association of CReMM/CHD9 with promoters in osteogenic cells. J Cell Physiol 207:374–378.

Sillibourne JE, Delaval B, Redick S, Sinha M, Doxsey SJ. 2007. Chromatin remodeling proteins interact with pericentrin to regulate centrosome integrity. Mol Biol Cell 9:3667–3680.

Stokes DG, Perry RP. 1995. DNA-binding and chromatin localization properties of CHD1. Mol Cell Biol 5:2745–2753.

Temtamy SA, McKusick VA. 1978. The genetics of hand malformations. New York: Alain R Liss, Inc. p. 619.

Thompson BA, Tremblay V, Lin G, Bochar DA. 2008. CHD8 is an ATP-dependent chromatin remodeling factor that regulates beta-catenin target genes. Mol Cell Biol 12:3894–3904.

Toyoda Y, Yanagida M. 2006. Coordinated requirements of human topo II and cohesin for metaphase centromere alignment under Mad2-dependent spindle checkpoint surveillance. Mol Biol Cell 17:2287–2302.

Vissers LE, van Ravenswaaij CM, Admiraal R, Hurst JA, de Vries BB, Janssen IM, van der Vliet WA, Huys EH, de Jong PJ, Hamel BC, Schoenmakers EFPM, Brunner HG, Veltman JA, van Kessel AG. 2004. Mutations in a new member of the chromodomain gene family cause CHARGE syndrome. Nat Genet 36:955–957.

Wakamatsu N, Kobayashi H, Miyatake T, Tsuji S. 1992. A novel exon mutation in the human beta-hexosaminidase beta subunit gene affects 3' splice site selection. J Biol Chem 267:2406–2413.

Woodage T, Basrai MA, Baxevanis AD, Hieter P, Collins FS. 1997. Characterization of the CHD family of proteins. Proc Natl Acad Sci USA 94:11472–11477.

Yamada Y, Goto H, Suzumori K, Adachi R, Ogasawara N. 1992. Molecular analysis of five independent Japanese mutant genes responsible for hypoxanthine guanine phosphoribosyltransferase (HPRT) deficiency. Hum Genet 90:379–384.

Yuan CC, Zhao X, Florens L, Swanson SK, Washburn MP, Hernandez N. 2007. CHD8 associates with human Staf and contributes to efficient U6 RNA polymerase III transcription. Mol Cell Biol 24: 8729–8738.

Congenital Anomalies
THE JAPANESE TERATOLOGY SOCIETY
doi:10.1111/j.1741-4520.2010.00282.x
Congenital Anomalies 2010; **50**, 197–199

CASE REPORT

Severe Peters Plus syndrome-like phenotype with anterior eye staphyloma and hypoplastic left heart syndrome: Proposal of a new syndrome

Reiko Shimizu[1], Ryota Saito[2], Kenji Hoshino[2], Kiyoshi Ogawa[2], Takashi Negishi[3], Jiro Nishimura[4], Norimasa Mitsui[5], Makiko Osawa[1], and Hirofumi Ohashi[5]

[1]Department of Pediatrics, School of Medicine, Tokyo Women's Medical University, Tokyo, and Divisions of [2]Cardiology, [3]Ophthalmology, [4]Plastic Surgery, and [5]Medical Genetics, Saitama Children's Medical Center, Saitama, Japan

ABSTRACT **Peters Plus syndrome is a very rare autosomal recessive condition characterized by ocular defects (typically Peters anomaly) and other systemic major/minor anomalies. Mutations in the *B3GALTL* gene encoding β 1,3-glucosyltransferase have been found in virtually all patients with typical Peters Plus syndrome. We report on a female patient with unusually severe manifestations of Peters Plus syndrome, including anterior eye staphyloma, cleft lip and palate, and hypoplastic left heart syndrome (HLHS). Analysis of the *B3GALTL* gene revealed no mutation in the patient. To our knowledge, HLHS has not previously been reported in Peters Plus syndrome so far, and anterior staphyloma, a most severe defect of the anterior eye chamber, is also apparently rare in the syndrome. Our patient might represent a new syndrome of severe Peters Plus syndrome-like phenotype with anterior eye staphyloma and HLHS.**

Key Words: anterior staphyloma, hypoplastic left heart syndrome, Peters anomaly, Peters Plus syndrome

INTRODUCTION

Peters Plus syndrome (MIM 261540) is a rare autosomal recessive disease characterized by ocular anterior chamber defects (typically Peters anomaly), distinctive facies (prominent forehead, hypertelorism, narrow palpebral fissure, long philtrum, cupid bow upper lip and malformed ears), cleft lip and palate, short hands and feet, and growth and developmental delay. Since the first detailed delineation of the syndrome by van Schooneveld *et al.* (1984), who coined the term 'Peters Plus syndrome', on the basis of 11 patients with anterior chamber cleavage defect and other multiple congenital anomalies, more than 60 patients have been reported to date. Recently, the syndrome was found to be caused by mutations in β1,3 glucosyltransferase like gene (*B3GALTL*) which codes for glucosyltransferase, β3Glc-T, suggesting that the syndrome is a glycosylation disorder (Lesnik Oberstein *et al.* 2006; Reis *et al.* 2008).

Congenital heart defects are occasionally found in the syndrome, at a frequency of around 30%, including atrial septal defect, ventricular septal defect, subvalvular aortic stenosis, pulmonary stenosis, and bicuspid pulmonary valve (Maillette de Buy Wenniger-Prick and Hennekam 2002). To our knowledge, however, hypoplastic left heart syndrome (HLHS) has not been previously described in the syndrome. Here we report a Japanese girl with Peters Plus syndrome-like phenotype and HLH. In addition, the patient had anterior eye staphyloma, a most severe developmental defect of the anterior eye chamber.

Correspondence: Reiko Shimizu, MD, PhD, Department of Pediatrics, School of Medicine, Tokyo Women's Medical University, 8-1 Kawada-cho, Shinjuku-ku, Tokyo 160-0022, Japan. Email: rmuto@ped.twmu.ac.jp

Received January 5, 2010; revised and accepted May 6, 2010.

CLINICAL DETAILS

The patient, a female, was born by normal delivery after an uneventful 37-week pregnancy to a 32-year-old, gravid 3, para 1, abortus 1 mother and a 34-year-old father, both Japanese, healthy and unrelated. No polyhydroamnios was noted in the pregnancy. The patient had a healthy elder brother. Her birth weight was 2390 g (−1.7 SD), length 46.2 cm (−1.4 SD) and occipitofrontal circumference (OFC) 32.0 cm (± 0 SD). Soon after birth, it was noticed that she had bilateral cleft lip and palate, and corneal opacity of both eyes. Other features also noted were a round face, a narrow forehead, hypertelorism, micrognathia, malformed ears, right preauricular pit, short broad hands, short fifth fingers with single flexion crease and hyperextensible finger joints (Fig. 1). No apparent rhizomelic limb shortening was noticed. Ophthalmological examination revealed anterior staphyloma of both eyes, lacking apparent anterior chamber structures (Fig. 2). On B-mode ultrasonography, both eyeballs were found to be small (around 12 mm), while optic nerves were normally observed.

The day after birth, the patient showed tachypnea and cyanosis and was admitted to our hospital on the suspicion of congenital heart defect. On admission, her weight was 2466 g (76 g gain in one day after birth) in spite of poor intake, heart rate 160/min, respiratory rate 70/min, and SpO_2 95% in room air. Cardiothoracic ratio (CTR) was 56% on a chest X-ray. Echocardiography revealed HLHS with aortic and mitral atresia and a large patent ductus arteriosus (Fig. 3). Despite intensive care, including prostaglandin E1 infusion, she died of ductal shock at the age of 15 days. A post-mortem autopsy was not granted and histopathological investigation for eyes was not performed. Although we could not perform thorough imaging studies, such as total skeletal survey and abdominal echography, no vertebral and urogenital anomalies were noted in the patient.

Chromosome analysis on lymphocytes revealed a normal 46, XX karyotype. Polymerase chain reaction (PCR) and direct sequencing analysis of the *B3GALTL* gene using genomic DNA obtained from residual peripheral blood used for chromosome analysis revealed no

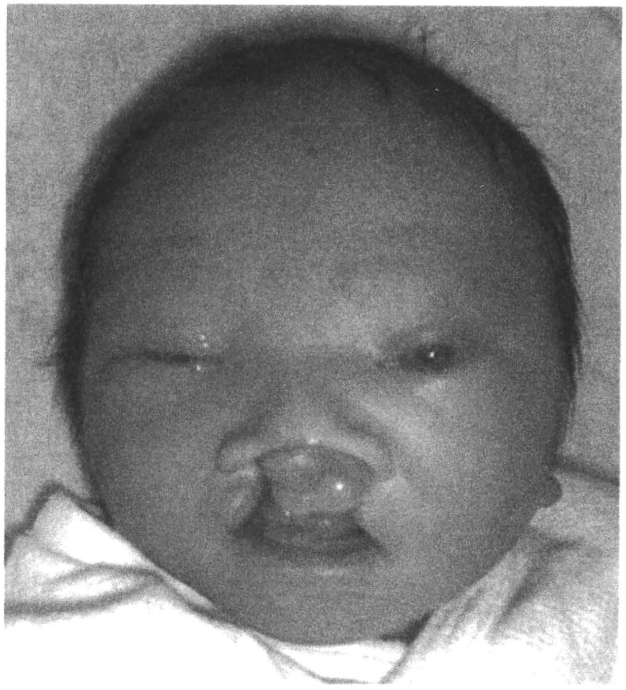

Fig. 1 Craniofacial view of the patient. (Permission for the presentation of this picture was obtained from the patient's parents.)

mutation in any exons or splice sites of the gene in the patient. Unfortunately, we could not perform further studies due to lack of specimen, such as array comparative genomic hybridization and multiplex ligation-dependent probe amplification to evaluate subtle genomic imbalance.

DISCUSSION

HLHS is a serious congenital heart defect characterized by severe underdevelopment of the left side heart structure with a prevalence of 1.4–3.8% among all congenital heart defects. The cause is unknown but is believed to be related to altered blood flow in cardiac embryogenesis leading to obstruction of the left side of the heart (Towbin *et al.* 1999). At least 10% of patients die within one week, and all patients without treatment die in the first year of life. HLHS is known to be occasionally associated with the following genetic entities: (i) Mendelian disorders: Apert syndrome, Holt-Oram syndrome, Ellis-van Creveld syndrome, Smith-Lemi-Opitz syndrome, Beckwith-Wiedemann syndrome, CHARGE syndrome, DiGeorge syndrome, Heterotaxy, Allagile syndrome, Rubinstein-Taybi syndrome, short rib-polydactyly syndrome type 3, PAGOD syndrome (Natowicz *et al.* 1988; Hanauer *et al.* 2002; Robert *et al.* 2007); (ii) Chromosomal abnormalities (including microdeletion syndromes): trisomy 13, trisomy 18, Turner syndrome, 7q35 deletion, Jacobsen syndrome and 16q24 deletion (Grossfeld 1999; Sedmera *et al.* 2005); and (iii) Non-Mendelian disorders: Sirenomelia sequence (Kim *et al.* 2007). However, a search of English-language publications failed to find any cases of Peters Plus syndrome associated with HLHS.

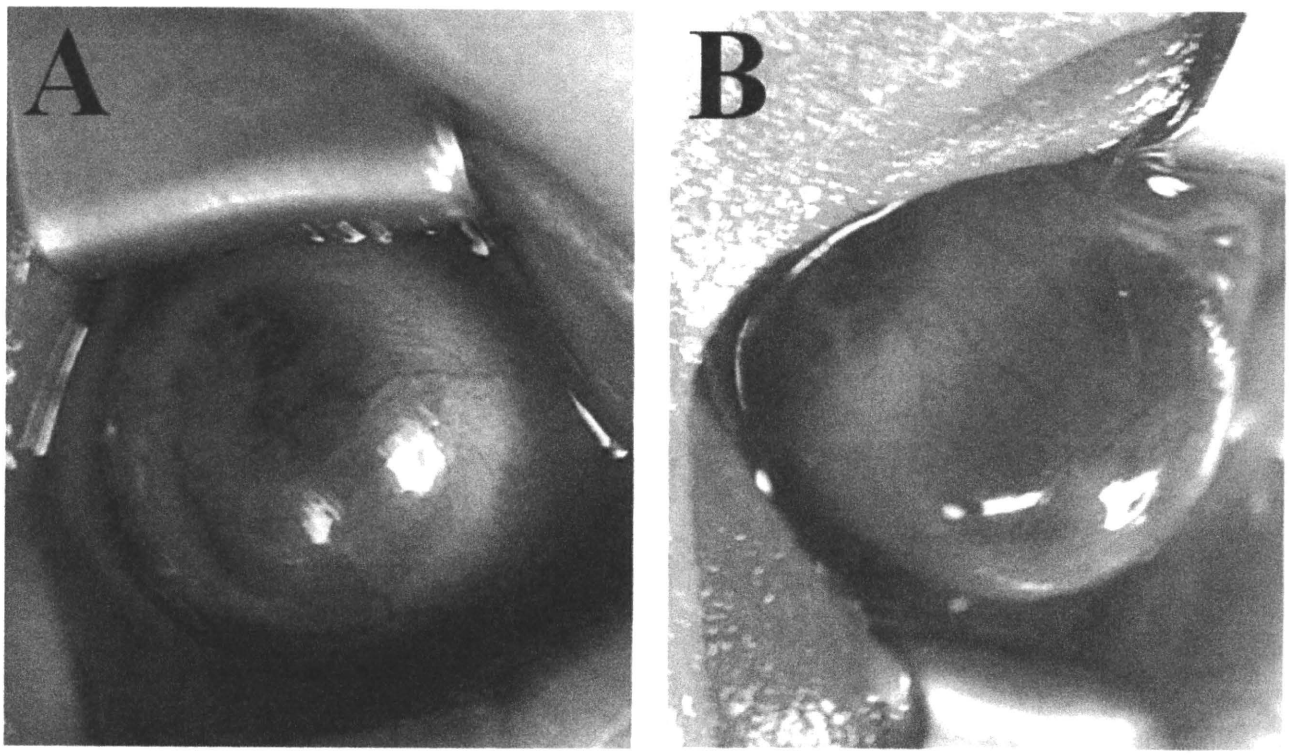

Fig. 2 Anterior staphyloma of both eyes. (A) Right eye. (B) Left eye.

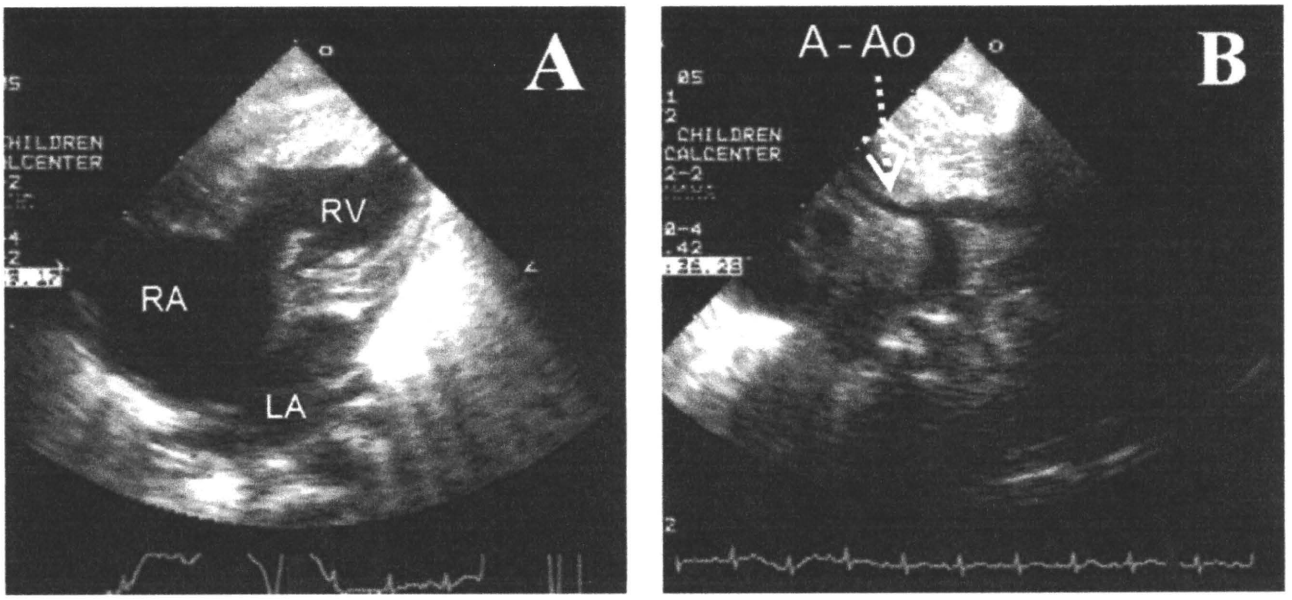

Fig. 3 Echocardiographic image of the patient. (A) Apical four-chamber view. Note hypoplastic left ventricle. (B) Suprasternal sagittal view. Note narrow ascending aorta of less than 1.5 mm in diameter. A-Ao, ascending aorta; LA, left atrium; RA, right atrium; RV, right ventricle.

Analysis of *B3GALTL* gene mutation status in two previous studies revealed the exclusively constant c.660 + 1G > A mutation in exon 8. Of 19 patients (or families) studied, homozygous c.660 + 1G > A mutation was found in 15 patients, and the remaining four patients were compound heterozygotes for the common c.660 + 1G > A mutation and for another mutation, c.230insT, c.347 + 5G > A, c.459 + 1C > A, and entire gene deletion, respectively (Lesnik Oberstein *et al.* 2006; Reis *et al.* 2008). It is noteworthy that mutations were found in all these typical patients.

The most characteristic feature of Peters Plus syndrome is Peters anomaly of the anterior eye chamber characterized by central corneal opacity (leukoma), thinning of the posterior aspect of the cornea, and iridocorneal adhesions, which are observed in 73% of patients (Maillette de Buy Wenniger-Prick and Hennekam 2002). The remaining patients have less severe anterior chamber manifestations, such as posterior embryotoxon. However, anterior staphyloma (ectasia of the cornea usually covered on the posterior surface by remnants of anteriorly displaced iris) present in our patient, a most severe expression of anterior chamber maldevelopment, is apparently rare in the syndrome.

As mentioned above, our patient showed unusual features of Peters Plus syndrome, such as HLHS and anterior staphyloma. Although we failed to identify similar previously published cases, an extensive search of non-English (Japanese) publications revealed a case similar to our patient. Nozaki *et al.* (1996) reported a 25-day -old Japanese boy who had anterior staphyloma in his left eye and HLHS. The cornea in his left eye was protruding and diffusely clouded and no recognizable anterior chamber structures were present, while hyperplasia of the iris stroma was noted in the right eye. Other features also described were congenital teeth, high arched palate, low-set ears and retained testes.

In conclusion, our patient and the patient reported by Nozaki *et al.* (1996) might represent a new syndrome of severe Peters Plus syndrome-like phenotype with anterior eye staphyloma and HLHS. The fact that no *B3GALTL* mutation was found in our patient also suggests this notion.

ACKNOWLEDGMENT

This work was partly sponsored by a grant from the Ministry of Health, Labour and Welfare, Japan.

REFERENCES

Grossfeld PD (1999) The genetics of hypoplastic left heart syndrome. *Cardiol Young* **9**: 627–632.

Hanauer D, Argilla M, Wallerstein R (2002) Rubinstein-Taybi syndrome and hypoplastic left heart. *Am J Med Genet* **112**: 109–111.

Kim JB, Park JJ, Ko JK *et al.* (2007) A case of PAGOD syndrome with hypoplastic left heart syndrome. *Int J Cardiol* **114**: 270–271.

Lesnik Oberstein SA, Kriek M, White SJ *et al.* (2006) Peters Plus syndrome is caused by mutations in B3GALTL, a putative glycosyltransferase. *Am J Hum Genet* **79**: 562–566.

Maillette de Buy Wenniger-Prick LJ, Hennekam RC (2002) The Peters' Plus syndrome: a review. *Ann Genet* **45**: 97–103.

Natowicz M, Chatten J, Clancy R *et al.* (1988) Genetic disorders and major extracardiac anomalies associated with the hypoplastic left heart syndrome. *Pediatrics* **82**: 698–706.

Nozaki M, Shirai S, Ozeki H, Majima A (1996) A case of Peters' anomaly with systemic malformations. *Rinsho Ganka* **50**: 1307–1311.

Reis LM, Tyler RC, Abdul-Rahman O *et al.* (2008) Mutation analysis of B3GALTL in Peters Plus syndrome. *Am J Med Genet A* **146A**: 2603–2610.

Robert ML, Lopez T, Crolla J *et al.* (2007) Alagille syndrome with deletion 20p12.2-p12.3 and hypoplastic left heart. *Clin Dysmorphol* **16**: 241–246.

van Schooneveld MJ, Delleman JW, Beemer FA, Bleeker-Wagemakers EM (1984) Peters' Plus: a new syndrome. *Ophthalmic Paediatr Genet* **4**: 141–145.

Sedmera D, Cook AC, Shirali G, McQuinn TC (2005) Current issues and perspectives in hypoplasia of the left heart. *Cardiol Young* **15**: 56–72.

Towbin JA, Casey B, Belmont J (1999) The molecular basis of vascular disorders. *Am J Hum Genet* **64**: 678–684.

Int J Oral-Med Sci 9(2):101-107, 2010

Original Article

A Comparison between Two-Dimensional and Three-Dimensional Cephalometry on Lateral Radiographs and Multi-Detector Row Computed Tomography of Human Skulls

Norimitsu Hirai,[1] Takahiro Yamauchi,[2] Kensuke Matsune,[2] Ryosuke Kobayashi,[1] Hitoshi Yabe,[3] Hirofumi Ohashi,[4] and Takahide Maeda[2]

[1]Nihon University Graduate School of Dentistry at Matsudo, Pediatric Dentistry, Matsudo, Chiba 271-8587, Japan
[2]Department of Pediatric Dentistry, Nihon University School of Dentistry at Matsudo, Matsudo, Chiba 271-8587, Japan
Divisions of [3]Radiology, and [4]Medical Genetics, Saitama Children's Medical Center, Iwatsuki, Saitama 339-8551, Japan

Correspondence to :
Norimitsu Hirai
E-mail : mano07011@g.nihon-u.ac.jp

Abstract

Proper understanding of the orofacial development and deformities associated with various syndromes is important for planning appropriate dental treatment and improving the craniofacial features. However, it is quite difficult to take cephalometric radiographs of patients with severe mental retardation or behavioral disorders, since patient co-operation and stability of body movement are necessary while taking the radiographs. Computed tomography (CT) is potentially a better tool for the diagnosis and treatment planning of complex maxillofacial deformities than conventional lateral cephalograms. CT images of patients with mental retardation can be taken under general anesthesia. The absorbed dose of radiation in 128 slice multi-detector row computed tomography (MDCT) used in this study is established as CTDI vol. 17.24 mGy, which is less than that of conventional CT (65 mGy). However, the use of MDCT for cephalometric analysis in pediatric dentistry has not been reported. Hence, the aim of the present study was to compare the reliability and difference of angle and linear measurements of craniofacial form using the landmarks on conventional and MDCT lateral cephalograms of human skulls. The results of this study showed that angular and linear measurements recorded from conventional and MDCT lateral cephalograms were similar. In conclusion, there were no significant differences in the mean and standard deviation of angular and linear measurements between conventional and MDCT lateral cephalograms of human skulls. Angular and linear analysis on MDCT cephalogram might show good precision for craniofacial analysis.

Keywords :
128 multi-detector row computed tomography, lateral cephalogram, angular analysis, linear analysis

Introduction

Since 1931, lateral cephalometric radiographs have been used for analyzing both maxillofacial and orthodontic deformities, and especially to evaluate growth in pediatric dentistry (1, 2). Proper understanding of the orofacial development and deformities associated with various syndromes is important for planning appropriate dental treatment and improving the craniofacial features. However, it is quite difficult to take cephalometric radiographs of patients with severe mental retardation or behavioral disorders, since patient co-operation and stability of body movement are necessary while taking the radiographs.

Computed tomography (CT) provides detailed information regarding the landmarks through sliced images. In modern medical CT, the x-ray source rotates within the gantry chamber that houses the x-ray tube and detector while the patient is being moved through the gantry on a bed ; this method of

CT scanning is known as helical CT and is the most widely used (3). CT, therefore, is potentially a better tool in the diagnosis and treatment planning of complex maxillofacial deformities than conventional cephalometrics (4). Furthermore, it is possible to take CT images of patients with mental retardation under general anesthesia.

Spiral CT, however, places a great biological burden on the patient because of its high radiation exposure. As radiation has a cumulative effect on the human body, any reduction in exposure to radiation is considered beneficial. With the recent introduction of cone-beam CT specifically designed for volumetric imaging of the maxillofacial area, the radiation dose to the patient is significantly reduced, which effectively reduces the exposure time and simultaneously reduces the absorbed radiation to the patient (5).

In recent years, cone beam CT technology has become more popular. Cone beam CT scan exposes the patient to less radiation than multi-detector row CT (6). The absorbed dose of x-ray in 128 multi-detector row computed tomography (MDCT) used in this study is established as CTDI vol. 17.24 mGy, which is less than that of conventional CT (65 mGy). Chest CT is the most sensitive diagnostic imaging modality for detection of lung cancer and the treatment of any equivocal abnormalities detected on chest radiographs (7, 8). With spiral CT and, more recently, multi-detector row CT techniques, the sensitivity for detection of lung cancer and pulmonary nodules has improved, and the best method of assessing tumor response in most clinical situations is MDCT, which can detect a large number of lesions with smaller diameters and has more precision on measuring when compared with other methods (9).

The craniofacial characteristics of many syndromes are still unknown because of the difficulty of obtaining stable images by conventional lateral cephalograms. CT is beneficial for patients who have craniofacial anomalies and orofacial clefts, or patients requiring orthognathic surgery. The use of MDCT for lateral cephalometric analysis has not been reported in pediatric dentistry. Therefore, the authors compared conventional and MDCT lateral cephalograms. To obtain accurate angle and linear data from two-dimensional images, positioning of the patient is of utmost importance, whereas positioning of the patient is not critical when recording three-dimensional images (10).

Hence, the aim of the present study was to compare the reliability and difference of angle and linear measurements of craniofacial form using the landmarks on conventional and MDCT lateral cephalograms of human skulls.

Materials and Methods

Six dry human skulls were obtained from the Department of Oral Anatomy, Nihon University School of Dentistry at Matsudo. In order to confirm the differences of linear and angle measurements in different developmental stages, skulls with three types of dentition were selected as follows: Phantom 1 with primary dentition, Phantoms 2 and 3 with mixed dentition, and Phantoms 4, 5 and 6 with permanent dentition. All skulls had normal occlusion and no deformity of craniofacial pattern. The mandibular position was fixed with adhesive tape from the ipsilateral temporal bone around the horizontal ramus of the mandible to the contralateral temporal bone.

Imaging protocol

Each phantom was positioned in the Cephalostat (AUTO III N CM: Asahi Roentogen) by fixing it between the ear rods. The ear rods were placed in the external acoustic meatus and the Frankfort horizontal plane was placed perpendicular to the floor. Lateral cephalograms were taken with the following radiographic settings, for all phantoms: 75 kV, 12 mA, 0.63 s. The phantoms were placed in MDCT of SOMATOM Definition AS+(SIEMENS) on a foam platform with the Frankfort horizontal plane perpendicular to the floor and the position of the center of SOMATOM was set using the midline light beam to coincide with the midsagittal plane. Six phantoms were scanned with MDCT, which acquires 128 slices per gantry rotation at a gantry rotation time of 500

ms. The imaging conditions of MDCT were as follows for all phantoms in the extended height mode: 120 kV ; 120 mAS ; resolution, 0.12～0.15 mm ; FOV, 180 mm～200 mm ; slice width, 38 mm ; helical pitch (H.P.), 1.2 mm ; exposure time, 4.18 s ; window width ; 1500 ; window level, 450 ; absorbed dose, CTDI vol. 17.24 mGy.

Lateral cephalometric radiographs

For the lateral cephalometric analysis, 19 landmarks with Frankfort plane based on the anatomical Porion were identified. Based on Down's analysis for Japanese, angle and linear measurements for phantoms with primary and mixed dentition, and permanent dentition were recorded on both images. On conventional cephalograms, the authors measured the angle between three landmarks using a protractor having a minimum unit of 0.5° and the linear dimensions between two landmarks using a 1/20 mm caliper. Each measurement was repeated three times. On MDCT images and conventional cephalograms, the same examiner marked 19 landmarks and measured angle and linear dimensions three times with a time interval of 1 day. All measured data in MDCT images were calculated by Syngo fastview (standalone viewing tool for DICOM images) software in each phantom. The identified cephalometric hard tissue landmarks were set by the same dentist who had 5 years clinical experience with conventional and MDCT lateral cephalograms. In the MDCT cephalograms, the linear values recorded were calculated as the data based on the scale bar in each image. In linear analysis of the conventional cephalograms, as the image was 1.1 times larger than the true measurement (11), the data obtained were divided by 1.1. Fig. 1 indicates the landmarks on conventional and MDCT cephalograms.

Statistical analysis

The mean value and standard deviation of angle and linear analyses in six phantoms on conventional and MDCT lateral cephalograms were statistically analyzed by Paired t-test.

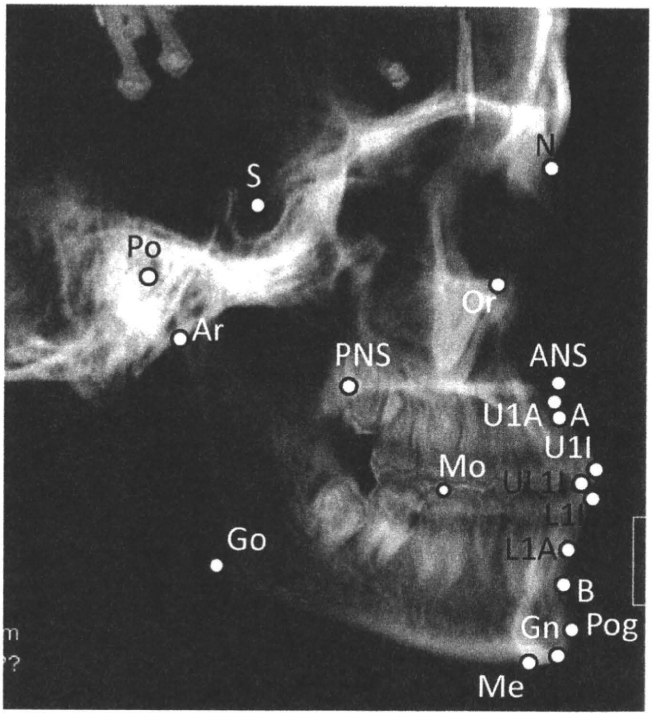

Fig. 1. Cephalometric image of MDCT

Results

In the present study, the intraobserver errors of angular analysis in conventional and MDCT lateral cephalograms (Fig. 1) were within 2.1 and 0.6° at Upper 1 to FH plane, respectively, on Phantom 1 with primary dentition (Table 1). On Phantom 6 with permanent dentition, the intraobserver errors were within 0.8° at FH to Upper 1 in both images (Table 2).

No significant differences in angular analysis were shown between conventional and MDCT cephalograms on Phantoms 1, 2, 3 with primary and mixed dentition. (Table 3), and Phantom 4, 5 and 6 with permanent dentition (Table 4).

The results of linear analysis of lateral cephalograms in conventional and MDCT images of Phantom 1 with primary dentition are shown in Table 5, and those of Phantom 6 with permanent dentition are indicated in Table 6. The intraobserver errors of linear analysis in two images were 0.1 mm to 0.4 mm on conventional and 0.1 mm on MDCT lateral cephalograms on Phantom 1, and were within 0.6 mm in both cephalograms on Phantom 6 (Tables 5 and 6).

Tables 7 and 8 show the average linear dimensions

Table 1. Angular analysis on conventional and MDCT cephalogram of Phantom 1 with primary dentition

	Conventional			MDCT		
Angular analysis	mean	SD	σi	mean	SD	σi
Skeletal						
Convexity	8.7	0.5	0.6	8.7	0.2	0.3
A-B plane	−5.8	0.2	0.3	−5.8	0.2	0.3
SNA	78.3	0.5	0.6	78.5	0.4	0.5
SNB	73.3	0.5	0.6	73.5	0.4	0.5
Facial angle	85.0	0.4	0.5	84.8	0.2	0.3
SNP	73.8	0.5	0.6	74.0	0.4	0.5
Y axis	58.2	0.2	0.3	58.3	0.2	0.3
SN-S·Gn	69.3	0.6	0.8	69.2	0.2	0.3
Mandibular plane	27.2	0.2	0.3	27.3	0.2	0.3
Gonial angle	127.2	0.2	0.3	127.3	0.2	0.3
GZN	90.3	0.2	0.3	90.2	0.2	0.3
FH to SN	11.2	0.5	0.6	11.0	0.0	0.0
Denture						
U-A to FH plane	100.7	1.7	2.1	100.7	0.5	0.6
U-A to SN plane	90.0	0.8	1.0	89.8	0.2	0.3
L-1 to Mandibular	81.5	1.5	1.8	81.7	0.5	0.6
Interincisal	150.5	0.4	0.5	150.3	0.5	0.6
Occlusal plane	9.7	0.9	1.2	9.8	0.2	0.3

SD; standard deviation, σi; intraobserver errors

Table 2. Angular analysis on conventional and MDCT cephalogram of Phantom 6 with permanent dentition

	Conventional			MDCT		
Angular analysis	mean	SD	σi	mean	SD	σi
SN to FH	13.8	0.2	0.3	14.0	0.4	0.5
SN to Palatal	10.8	0.2	0.3	11.0	0.4	0.5
SN to Mandibular	25.2	0.2	0.3	25.2	0.2	0.3
FH to Occlusal	6.2	0.2	0.3	6.2	0.2	0.3
FH to Mandibular	11.3	0.2	0.3	11.0	0.4	0.5
SNA	81.0	0.0	0.0	81.0	0.0	0.0
FH to NA	94.7	0.2	0.3	94.7	0.2	0.3
Convexity	−3.7	0.2	0.3	−3.8	0.2	0.3
SNB	82.0	0.0	0.0	82.2	0.2	0.3
SN Pog	82.5	0.0	0.0	82.8	0.2	0.3
FH to NB	95.8	0.2	0.3	95.7	0.2	0.3
Facial angle	96.8	0.2	0.3	97.0	0.0	0.0
Y axis	51.0	0.0	0.0	50.8	0.2	0.3
Gonial angle	112.5	0.4	0.5	112.8	0.2	0.3
ANB	−1.0	0.0	0.0	−1.2	0.2	0.3
Palatal to Mandibular	14.2	0.2	0.3	14.0	0.4	0.5
FH to Upper 1	125.0	0.4	0.5	125.2	0.6	0.8
FH to Lower 1	78.0	0.4	0.5	77.8	0.2	0.3
Interincisal	132.8	0.2	0.3	132.5	0.4	0.5
Mandibular to Lower 1	90.3	0.2	0.3	90.7	0.2	0.3

SD; standard deviation, σi; intraobserver errors

Table 3. Average of angular analysis on conventional and MDCT cephalograms of three phantoms with one primary and two mixed dentition

	Conventional		MDCT		
	mean	SD	mean	SD	*t*-test
Skeletal					
Convexity	11.7	2.1	11.6	2.1	1.0
A-B plane	−8.1	1.6	−8.3	1.9	0.9
SNA	79.3	1.7	79.8	1.6	0.8
SNB	73.1	0.9	73.4	0.7	0.7
Facial angle	82.8	2.1	82.7	2.2	1.0
SNP	73.6	0.9	73.8	0.8	0.8
Y axis	60.9	2.8	62.0	2.9	0.7
SN-S·Gn	70.3	1.5	70.2	1.4	0.9
Mandibular plane	29.0	4.0	29.9	3.7	0.8
Gonial angle	128.5	3.4	128.3	3.1	1.0
GZN	89.5	0.5	89.3	0.8	0.8
FH to SN	9.3	1.6	8.9	1.9	0.8
Denture					
U-1(A) to FH plane	100.8	7.8	100.4	8.2	1.0
U-1(A) to SN plane	92.2	8.5	92.2	8.8	1.0
L-1 to Mandibular	87.9	5.0	88.1	4.6	1.0
Interincisal	141.4	13.5	140.9	13.8	1.0
Occlusal plane	14.6	3.7	15.7	4.3	0.8

$p<0.05$ SD; standard deviation

Table 4. Average of angular analysis on conventional and MDCT cephalograms of three phantoms with permanent dentition

	Conventional		MDCT		
	mean	SD	mean	SD	*t*-test
SN to FH	11.4	1.8	11.1	2.1	0.9
SN to Palatal	9.5	2.0	9.1	2.3	0.8
SN to Mandibular	27.2	3.1	27.3	2.5	1.0
FH to Occlusal	6.7	0.7	6.6	0.8	0.8
FH to Mandibular	16.3	4.6	16.1	4.2	1.0
SNA	82.8	1.9	83.1	1.5	0.9
FH to NA	94.0	0.3	94.3	0.3	0.4
Convexity	6.1	7.1	5.9	7.0	1.0
SNB	79.7	1.8	79.8	1.8	1.0
SN Pog	80.5	1.5	80.7	1.7	0.9
FH to NB	90.8	3.4	90.9	3.5	1.0
Facial angle	91.7	3.3	92.1	3.6	0.9
Y axis	55.4	3.3	55.5	3.3	1.0
Gonial angle	115.9	9.6	116.1	8.9	1.0
ANB	3.1	3.7	3.4	3.3	0.9
Palatal to Mandibular	17.9	5.0	17.8	4.4	1.0
FH to Upper 1	116.9	6.3	116.9	5.9	1.0
FH to Lower 1	65.9	9.3	65.3	9.1	1.0
Interincisal	128.6	4.3	128.3	4.2	1.0
Mandibular to Lower 1	97.9	5.0	98.2	5.4	1.0

$p<0.05$ SD; standard deviation

Table 5. Linear analysis in conventional and MDCT cephalogram of Phantom 1 with primary dentition

	Conventional			MDCT		
	mean	SD	σi	mean	SD	σi
S-N	55.8	0.1	0.1	56.6	0.0	0.0
ANS-PNS	39.5	0.3	0.4	39.9	0.0	0.1
Go-Me	46.2	0.2	0.2	46.9	0.0	0.0
S-Go	48.9	0.1	0.1	48.8	0.1	0.1
N-Pog	79.6	0.1	0.2	79.8	0.1	0.1
Or-ANS	18.3	0.3	0.4	17.7	0.1	0.1

SD ; standard deviation, σi ; intraobserver errors

Table 6. Linear analysis on conventional and MDCT cephalogram of Phantom 6 with permanent dentition

	Conventional			MDCT		
	mean	SD	σi	mean	SD	σi
S-N	60.7	0.1	0.2	60.2	0.0	0.3
ANS-PNS	47.0	0.2	0.2	46.2	0.6	0.6
Go-Me	68.6	0.2	0.3	68.1	0.0	0.1
S-Go	68.9	0.1	0.1	69.3	0.1	0.2
N-Pog	94.7	0.1	0.1	94.2	0.2	0.2
Or-ANS	23.7	0.1	0.1	23.3	0.4	0.2

SD ; standard deviation, σi ; intraobserver errors

Table 7. Average of linear analysis on conventional and MDCT cephalograms of three phantoms with one primary and two mixed dentition

	Conventional		MDCT		
	mean	SD	mean	SD	*t*-test
S-N	57.4	4.3	57.7	4.2	0.9
ANS-PNS	40.2	3.7	40.8	3.8	0.9
Go-Me	50.0	4.5	49.7	3.7	0.9
S-Go	53.0	4.5	52.5	4.3	0.9
N-Pog	84.4	9.3	84.7	9.2	1.0
Or-ANS	19.4	2.4	19.4	2.5	1.0

$p<0.05$ SD ; standard deviation

Table 8. Average of linear analysis on conventional and MDCT cephalograms of three phantoms with permanent dentition

	Conventional		MDCT		
	mean	SD	mean	SD	*t*-test
S-N	61.6	0.9	61.8	1.5	0.9
ANS-PNS	49.9	3.1	50.0	4.0	1.0
Go-Me	65.1	7.5	64.6	7.1	0.9
S-Go	69.3	5.0	69.7	5.0	0.9
N-Pog	96.6	3.4	96.4	4.0	1.0
Or-ANS	26.4	3.6	26.6	4.0	0.9

$p<0.05$ SD ; standard deviation

in conventional and MDCT lateral cephalograms in primary/mixed dentition and permanent dentition, respectively. The mean and standard deviation of linear dimensions in primary/mixed dentition and permanent dentition in conventional and MDCT lateral cephalograms were similar, and showed no significant difference.

Discussion

Recently, the application of three-dimensional (3D) lateral CT images is becoming more popular in the field of pediatric dentistry. Especially in mentally retarded patients, it is difficult to take conventional two-dimensional (2D) lateral and frontal cephalograms. However, evaluation of craniofacial development and symmetry is necessary to determine the craniofacial characteristics and plan appropriate treatment. Regardless of the type of CT used, the images produced by CT method allow better localization of the anatomical structures than conventional 2D radiographs, which are often geometrically distorted and plagued by bilateral structural superimpositions (12). Van Vlijmen *et al.* (13) reported that the position of the patient plays an important role in the outcome of cephalometric analysis because the measurements are influenced by tilt or rotations of the head. The position of the patient in CT scanner is not that important for 3D angular and linear measurements because rotation along the long axis or the sagittal axis is not of any influence. CT is potentially a better tool for the diagnosis and treatment planning of the complex maxillofacial deformities than conventional cephalograms (14).

Spiral CT, however, places a high economic and biological burden on the patient because of its high cost and radiation exposure. As radiation has a cumulative effect on the human body, any reduction in exposure to radiation is considered beneficial. The

new MDCT reduces exposure time and simultaneously reduces the radiation absorbed by the patient (15, 16). The MDCT-derived 3D cephalogram has a number of potential advantages over conventional CT, including sub-millimeter resolution and reduced radiation exposure, while still permitting reconstruction of the soft tissue profile. However, landmarks should be marked accurately on images for cephalometric analysis. In some cases, it is quite difficult to locate the landmarks, thus leading to an incorrect diagnosis. The main reason for errors in cephalometric studies is errors in landmark identification (17). Landmark identification is essential not only on conventional but also on MDCT lateral cephalograms. Williams and Richtsmeier (18) studied the reliability of 28 skeletal mandibular landmarks and the accuracy of 378 linear distances formed by the landmarks on 3D spiral CT images, and the mean accuracy of all linear distances was 0.377 ± 1.136 mm with a range of 0.001 to 3.889 mm, and approximately 58% of measurements were less than 1.0 mm from true values. They concluded that MDCT proved to be slightly more accurate than cone beam CT. Lou *et al.* (14) reported that for the conventional landmarks used in lateral and frontal cephalograms, there was no evidence to indicate that 3D spiral CT was more reliable than cephalometric methods. They stated that 3D CT should be reserved for severe asymmetric craniofacial cases. In a study by Mischkowski *et al.* (19), 30 holes with a diameter of 0.6 mm were drilled with a surgical drill in defined positions in the maxillofacial area of a dry human skull and all distances were measured manually with a precision digital caliper. They compared these values with measurements recorded by cone-beam CT (CBCT) and MDCT. The authors concluded that linear distance measurements revealed an average absolute error of 0.26 ± 0.18 mm for CBCT scanner and of 0.18 ± 0.17 mm for the MDCT scanner, which were not statistically significant. Slight differences of some of the linear measurements on conventional and MDCT lateral cephalograms were observed, however, which were similar to those reported by Cavalcanti *et al.* (20). This difference was most likely due to the discord between 2D and 3D images in which landmarks were identified. However, these differences probably do not translate into clinical relevance.

In the present study, the intraobserver errors of angular and linear analysis in conventional and MDCT lateral cephalograms were small in primary, mixed and permanent dentitions. The difference of angular and linear analysis between conventional and MDCT cephalograms was not significant.

From this study, it is suggested that MDCT cephalograms might be clinically accurate for craniofacial analyses.

Conclusion

Angular and linear measurements in conventional and MDCT lateral cephalograms were similar. The differences of data in each angular and linear measurement between conventional and MDCT cephalometry were within an angle of 1.1° and a length of 0.6 mm, respectively.

In conclusion, no significant differences were found in the mean and standard deviation of angular and linear measurements between conventional and MDCT lateral cephalograms in six skulls. The angular and linear analysis on MDCT cephalograms might be clinically accurate for craniofacial analysis.

Acknowledgments

The authors would like to thank Prof. T. Kaneda, Department of Radiology, for his valuable advice and Prof. E. Kanazawa, Department of Anatomy and Physical Anthropology, for his continuous and kind support.

This study was funded in part by a Grant for the Support of Projects for Strategic Research at Private Universities by the Ministry of Education, Culture, Sports, Science and Technology (MEXT), 2008-2012.

References

1. Broadbent BH : A new technique and its application to orthodontia. Angle Orthod, 1 : 45-66, 1931.
2. Gottlieb EL, Nelson AH, Vogels DS : 1990 JCO study

of orthodontic diagnosis and treatment procedures 1 Results and trends. J Clin Orthod, 25 : 145-156, 1991.
3. Hounsfield GN : Computerized transverse axis scanning (tomography) Part 1 Description of system. Br J Radiol, 68 : 166-172, 1995.
4. Carlsson CA : Imaging modalities in x-ray computerized tomography and in selected volume tomography. Phy Med Bio, 44 : 23-56, 1999.
5. Mah JK, Danforth RA, Bumann A, Hatcher D : Radiation absorbed in maxillofacial imaging with a new dental computed tomography device. Oral Surg Oral Med Oral Pathol Oral Radiol Endod, 96 : 508-513, 2003.
6. Ludlow JB, Ivanovic M : Comparative dosimetry of dental CBCT devices and 64-slice CT for oral and maxillofacial radiology. Oral Surg Oral Med Oral Pathol Oral Radiol Endod, 106 : 106-114, 2008.
7. Heitzman ER : The role of computed tomography in the diagnosis and management of lung cancer, an overview. Chest, 89 : 237-241, 1986.
8. Henschke CI, McCauley DI, Yankelevitz DF, Naidich DP, McGuinness G, Miettinen OS, Libby DM, Pasmantier MW, Koizumi J, Altorki NK, Smith JP : Early Lung Cancer Action Project : overall design and findings from baseline screening. Lancet, 354 : 99-105, 1999.
9. Erasmus JJ, Gladish GW, Broemeling L, Sabloff BS, Truong MT, Herbst RS, Munden RF : Interobserver and intraobserver variability in measurement of non-small-cell carcinoma lung lesions : implications for assessment of tumor response. J Clin Oncol, 21 : 2574-2582, 2003.
10. Swennen GRJ, Schutyser F, Hausamen JE, eds : Three dimensional cephalometry. A color atlas and manual. Berlin : Heidelberg Springer, 183-226, 2005.
11. Sebata M, Yamaguchi H : Morphological examination. In : Iizuka T, Sebata M, Iwasawa T, Motohashi Y. Orthodontics. Ishiyaku Shuppan ; 1992. p.169-171.
12. Salzmann JA : Limitation of roentgenographic cephalometrics. Am J Orthod, 50 : 169-188, 1964.
13. van Vlijmen OJ, Maal T, Bergé SJ, Bronkhorst EM, Katsaros C, Kuijpers-Jagtman AM : Comparison of cephalometric radiographs obtained from cone beam computed tomography scan and conventional radiographs. J Oral Maxillofac Surg, 67 : 92-97, 2009.
14. Lou L, Lagravere MO, Compton S, Major PW, Flores-Mir C : Accuracy of measurements and reliability of landmark identification with computed tomography (CT) techniques in the maxillofacial area : a systematic review. Oral Surg Oral Med Oral Pathol Oral Radiol Endod, 104 : 402-411, 2007.
15. Mozzo P, Procacci C, Tacconi A, Martini PT, Andreis IA : A new volumetric CT machine for dental imaging based on the cone-beam technique : preliminary results. Eur Radiol, 8 : 1558-1564, 1998.
16. Mah JK, Danforth RA, Bumann A : Radiation absorbed in maxillofacial imaging with a new dental computed tomography device. Oral Surg Oral Med Oral Pathol Oral Radiol Endod, 96 : 508-513, 2003.
17. Houston WJ : The analysis of errors in orthodontic measurements. Am J Orthod, 83 : 382-390, 1983.
18. Williams FL, Richtsmeier JT : Comparison of mandibular landmarks from computed tomography and 3D digitizer data. Clin Anat, 16 : 494-500, 2003.
19. Mischkowski RA, Pulsfort R, Ritter L, Neugebauer J, Brochhagen HG, Keeve E, Zöller JE : Geometric accuracy of a newly developed cone-beam device for maxillofacial imaging. Oral Surg Oral Med Oral Pathol Oral Radiol Endod, 104 : 551-559, 2007.
20. Cavalcanti MG, Vannier MW : Three dimensional computed tomography landmark measurement in craniofacial surgical planning : experimental validation in vitro. J Oral Maxillofac Surg, 57 : 690-694, 1999.

Int J Oral-Med Sci 9(2):108-114, 2010

Original Article

Accuracy of Tooth Development Stage, Tooth Size and Dental Arch width in Multi-Detector Row Computed Tomography of Human Skulls

Takahiro Yamauchi,[1] Norimitsu Hirai,[2] Kensuke Matsune,[1] Ryosuke Kobayashi,[2] Hitoshi Yabe,[3] Yasuo Takahashi,[4] Hirofumi Ohashi,[5] and Takahide Maeda[2]

[1]Department of Pediatric Dentistry, Nihon University School of Dentistry at Matsudo, Matsudo, Chiba 271-8587, Japan
[2]Nihon University Graduate School of Dentistry at Matsudo, Pediatric Dentistry, Matsudo, Chiba 271-8587, Japan
Divisions of [3]Radiology, [4]Pediatric Dentistry, and [5]Medical Genetics, Saitama Children's Medical Center, Iwatsuki, Saitama 339-8551, Japan

Correspondence to :
Norimitsu Hirai
E-mail : mano07011@g.nihon-u.ac.jp

Keywords :
128 multi-detector row computed tomography, tooth development stage, tooth size, dental arch width

Abstract
In pediatric dentistry, examination of the development of crown or tooth root is essential to determine the physiological development age. Measurements of the tooth size and dental arch width are also required to predict normal occlusion and oral function, and to plan appropriate dental treatment. Some dental anomalies are keys to identify congenital malformation syndromes. In patients with behavioral disorders, it is quite difficult to take diagnostic dental models and pantomographs, since patient co-operation and stability in body movement for a few minutes is necessary while taking the dental impression and pantomographs. For patients with severe mental retardation and behavioral disorders, performing computed tomography under general anesthesia or deep sedation is easier than taking pantomographs while awake. The aim of the present study was to compare the tooth development stage on pantomographs and mesiodistal diameter measurements of tooth size and dental arch width of dry human skulls with the images of those on 128 multi-detector row computed tomography (MDCT). Based on the results, the measurements of tooth development stage, tooth size and dental arch width on MDCT images were clinically precise.

Introduction

In pediatric dentistry, examination of the tooth development is essential to determine the physiological development age (1, 2). Measurements of tooth size and dental arch width are also required to predict normal occlusion (3) and oral function, and to plan appropriate dental treatment. Some dental anomalies are keys to identify congenital malformation syndromes (4). For thorough examination, dental models and pantomographs are necessary. To evaluate the craniofacial growth in children, lateral cephalometry (5) and pantomography (6) have been utilized. Tooth size anomalies like macrodontia or microdontia, abnormalities in teeth numbers and dental arch width with narrowed arch or high arched palatal vault are important in the detection of some syndromes. However, in some patients with behavioral disorders, taking diagnostic dental models and pantomographs is quite difficult, since the patient must co-operate and remain stable for a few minutes while taking the dental impression and pantomographs. In these patients, taking a dental impression involves the risk of apnea. For patients with severe mental retardation and severe behavioral disorder, performing computed tomography (CT) under general anesthesia or deep sedation is easier than taking pantomographs while awake.

A medical CT system known as multi-detector row computed tomography has recently been developed and is now being applied for the diagnosis of tumors (7), external injuries (8) and in the dental field for clarifying the relationship between the lower

third molar and inferior canal (9). In comparison with conventional CT systems, multi-detector row CT allows rapid imaging with a smaller burden on the patient, and yields higher image quality while requiring a small exposure dose (10, 11).

In recent years, up-to-date CT technology including cone beam CT with less radiation than conventional CT has been increasing in popularity. Recently, the 128 multi-detector row computed tomography (MDCT) used in the present study gained attention, because the CT provides detailed and accurate three-dimensional construction images with less radiation than conventional CT. The best method of assessing tumor response in most clinical situations is MDCT, as it can detect a large number of lesions with smaller diameters and measurement is more precise when compared with other methods (12). No study has compared the tooth development stage on conventional and MDCT pantomographs, and the tooth size and dental arch size on the skull and on the MDCT.

Hence, the aim of the study was to compare the tooth development stage of permanent teeth on pantomographs and mesiodistal diameter measurements of tooth size and dental arch width on the skull with MDCT images.

Materials and Methods

Six dry human skulls were obtained from the collection of the Department of Oral Anatomy and Physical Anthropology of Nihon University School of Dentistry at Matsudo. One skull (Phantom 1) with primary dentition, 2 skulls (Phantom 2 and Phantom 3) with mixed dentition and 3 skulls (Phantom 4, Phantom 5 and Phantom 6) with permanent dentition were used to estimate the tooth development of permanent teeth, and to measure the mesiodistal diameter of tooth size and dental arch width in primary, mixed and permanent dentitions. The mandibular position of phantoms was fixed with broad tape from the ipsilateral temporal bone around the horizontal ramus of the mandible to the contralateral temporal bone.

Imaging protocol

Each phantom was positioned in the cephalostat (AUTO IIIN CM : Ashahi Roentogen) by fixing it between the ear rods. The ear rods were placed in the external acoustic meatus and the Frankfort horizontal plane was placed perpendicular to the floor. For all phantoms, pantomographs were taken with the following radiographic settings : 75 kV, 12 mA, 0.63 s. The same phantoms were placed in MDCT of SOMATOM Definition AS+ (SIEMENS) on a foam platform with the Frankfort horizontal plane perpendicular to the floor and the position of the center of SOMATOM was set using the midline light beam to coincide with the midsagittal plane. The following imaging conditions were maintained for all phantoms in the extended height mode : 120 kV ; 120 mAS ; resolution, 0.12～0.15 mm ; FOV, 180 mm ～200 mm ; slice width, 38 mm ; helical pitch (HP), 1.2 mm ; exposure time, 4.18 s ; window width, 1500 ; and window level, 450.

Tooth developmental stage

Based on the criteria of Nolla (1), the developmental stage of each permanent tooth was evaluated on conventional and MDCT pantomographs using a set of drawings illustrating the 10 stages of the teeth by a pedodontist who had over 5 years of clinical experience.

Tooth size and dental arch width

Crown mesiodistal diameter and dental arch width were directly measured on the six phantoms three times using a 1/20 mm caliper by the same observer. Dental arch width was expressed as Wc and We which means the distance between the most distal corners of the left-right primary canines and primary second molars, respectively, and W3 and W6 means the distance between the most distal corners of left-right permanent canines and permanent first molars, respectively.

On MDCT images, one dentist evaluated the most mesial and distal corners of each tooth, and Wc, We, W3 and W6 were measured three times. All data were calculated by Syngo fastview (standalone view-

ing tool for DICOM images) software in each phantom. In MDCT images, crown mesiodistal diameters and dental arch widths were measured from converted data based on the scale bar which was calculated and fixed as a true distance in each image.

Statistical analysis

From the conventional and MDCT pantomographs, one dentist evaluated the tooth developmental stage and measured crown diameter and dental arch width three times with a time interval of 1 day. The data of tooth development stage on conventional and MDCT pantomographs were statistically compared by Wilcoxon rank sum test, and tooth size and dental arch width were analyzed by paired t-test.

Results

Tooth development stage

Comparison of the tooth developmental stage of each permanent tooth on conventional and MDCT pantomographs of Phantom 1 is shown in Table 1 and Fig. 1. The difference of the average intraobserver errors of tooth development stage on conventional and MDCT pantomographs of Phantom 1 was 0.3. Data from Phantoms 2 and 3 are not shown, because those phantoms were very similar to Phantom 1. The average tooth development stages of permanent teeth in maxilla on the MDCT pantomographs in Phantoms 1, 2 and 3 were significantly higher than those of conventional pantomographs ($P<0.05$). No significant difference, however, was seen the average stages of the teeth in mandible between conventional and MDCT pantomographs in Table 2.

Fig. 1. Tooth development stage of permanent teeth by MDCT Pantomograph

Tooth size and dental arch width

Mesiodistal diameters of each primary tooth and

Table 1. Tooth development stage in pantomograph and MDCT of Phantom 1 with primary dentition

	mean(RU)	SD	σi	mean(LU)	SD	σi	mean(RL)	SD	σi	mean(LL)	SD	σi
pantomograph												
1	5.0	0.0	0.0	5.0	0.0	0.0	6.0	0.0	0.0	6.0	0.0	0.0
2	4.7	0.5	0.6	4.7	0.5	0.6	5.7	0.5	0.6	5.7	0.5	0.6
3	4.3	0.5	0.6	4.3	0.5	0.6	4.3	0.5	0.6	4.3	0.5	0.6
4	2.0	0.8	1.0	2.0	0.8	1.0	3.5	0.0	0.0	3.5	0.0	0.0
5	2.0	0.0	0.0	2.0	0.0	0.0	2.0	0.0	0.0	2.0	0.0	0.0
6	4.7	0.5	0.6	5.0	0.0	0.0	5.7	0.5	0.6	5.3	0.5	0.6
7	0.0	0.0	0.0	0.3	0.5	0.6	1.0	0.0	0.0	2.0	0.0	0.0
CT												
1	5.7	0.5	0.6	5.7	0.5	0.6	7.2	0.0	0.0	7.2	0.0	0.0
2	5.7	0.5	0.6	5.7	0.5	0.6	7.2	0.0	0.0	7.2	0.0	0.0
3	4.7	0.5	0.6	4.7	0.5	0.6	6.0	0.0	0.0	6.0	0.0	0.0
4	4.0	0.0	0.0	4.0	0.0	0.0	4.3	0.5	0.6	4.3	0.5	0.6
5	2.7	0.5	0.6	2.7	0.5	0.6	2.7	0.5	0.6	2.7	0.5	0.6
6	6.0	0.0	0.0	6.0	0.0	0.0	6.0	0.0	0.0	6.0	0.0	0.0
7	1.0	0.0	0.0	1.0	0.0	0.0	1.0	0.0	0.0	3.0	0.0	0.0

RU ; Right upper, LU : Left upper, RL : Right lower, LL : Left lower SD ; standard deviation, σi ; intraobserver errors

Table 2. Tooth development stages of upper and lower central incisor to second premolar in phantom and CT findings

	pantomograph			CT	
	mean	SD		mean	SD
Upper(1-5)	5.42	2.19	*	6.33	1.84
Lower(1-5)	6.06	2.01	NS	6.81	1.88

* ; $P<0.05$
NS ; not significant

Table 3. Tooth size in the skull and MDCT of Phantom 1 with primary dentition

		Skull			CT		
	teeth	mean	SD	σi	mean	SD	σi
Right Upper	A	6.3	0.0	0.0	6.2	0.0	0.1
	B	5.0	0.1	0.1	5.0	0.1	0.1
	C	6.3	0.2	0.2	6.3	0.0	0.1
	D	6.5	0.1	0.1	6.3	0.3	0.4
	E	8.4	0.1	0.1	8.3	0.1	0.2
Right Lower	A	3.7	0.0	0.0	3.8	0.3	0.4
	B	4.2	0.1	0.1	4.4	0.2	0.3
	C	5.6	0.0	0.0	5.6	0.0	0.1
	D	8.0	0.0	0.0	7.9	0.2	0.3
	E	9.5	0.5	0.6	9.5	0.2	0.2

SD ; standard deviation, σi ; intraobserver eerors

Table 4. Tooth size in the skull and MDCT of Phantom 6 with permanent dentition

		Skull			CT		
	teeth	mean	SD	σi	mean	SD	σi
Right Upper	1	9.0	0.1	0.1	8.8	0.1	0.1
	2	7.3	0.0	0.0	7.2	0.2	0.2
	3	7.8	0.0	0.0	7.8	0.1	0.1
	4	6.3	0.1	0.1	6.2	0.2	0.2
	5	5.8	0.1	0.1	5.7	0.0	0.1
	6	10.2	0.2	0.2	10.0	0.4	0.6
	7	9.3	0.1	0.2	8.7	0.1	0.2
Right Lower	1	5.7	0.0	0.0	5.5	0.1	0.2
	2	6.6	0.0	0.0	6.6	0.1	0.2
	3	6.9	0.1	0.1	6.9	0.2	0.2
	4	6.4	0.1	0.1	6.3	0.2	0.3
	5	6.6	0.0	0.0	6.5	0.4	0.5
	6	10.6	0.1	0.2	10.7	0.2	0.2
	7	9.9	0.0	0.0	10.4	0.1	0.2

SD ; standard deviation, σi ; intraobserver errors

permanent tooth on Phantom 1 and Phantom 6 on their MDCT images are shown in Table 3 and Table 4, respectively. Phantoms 2, 3, 4 and 5 are not shown. The intraobserver errors of tooth size on phantoms and MDCT images of Phantom 1 and Phantom 6 were limited within 0.6 mm, and dental arch widths of Wc, W_E, W3 W6 were within 0.4 mm, 0.3, 0.3 and 0.2, respectively. The tooth size and dental arch

Table 5. Average of tooth size in the Skull and MDCT of 6 phantoms

	Skulls		CT			Skulls		CT		
tooth	mean(RU)	SD	mean(RU)	SD	*t*-test	mean(RL)	SD	mean(RL)	SD	*t*-test
1	8.6	0.3	8.6	0.3	0.9	5.1	0.3	5.2	0.3	0.7
2	6.5	0.5	6.6	0.5	0.7	5.6	0.7	5.6	0.7	0.9
3	7.4	0.4	7.4	0.3	1.0	6.4	0.4	6.5	0.4	0.8
4	6.1	0.2	6.3	0.2	0.3	6.4	0.2	6.5	0.1	0.5
5	5.9	0.6	5.9	0.6	0.9	6.4	0.4	6.4	0.3	0.8
6	10.1	0.4	10.3	0.3	0.1	10.6	0.2	10.7	0.2	0.4
7	9.7	0.6	9.6	0.6	0.7	10.0	0.5	9.7	0.5	0.2
8	8.7	0.6	8.7	0.6	0.9	10.0	0.4	10.1	0.4	0.9
A	6.2	0.0	6.2	0.2	0.4	3.9	0.3	3.9	0.2	0.8
B	5.0	0.1	4.9	0.1	0.5	4.5	0.2	4.4	0.2	0.3
C	6.6	0.4	6.7	0.4	0.9	5.8	0.2	5.9	0.2	0.7
D	6.4	0.4	6.3	0.5	0.5	7.9	0.2	7.9	0.1	0.3
E	8.7	0.7	9.0	0.5	0.4	9.8	0.5	9.8	0.6	0.7

RU ; Right upper, RL ; Right lower $p<0.05$ SD ; standard deviation

Table 6. Dental arch width in Skull and MDCT of Phantom 1 with primary dentition

	Skull			CT		
	mean	SD	σi	mean	SD	σi
Upper Wc	31.1	0.2	0.2	31.0	0.1	0.2
WE	42.3	0.2	0.3	42.8	0.1	0.2
Lower Wc	25.2	0.1	0.1	24.9	0.3	0.4
WE	41.0	0.2	0.2	41.6	0.2	0.3

SD ; standard deviation, σi ; intraobserver errors

Table 7. Dental arch width in Skull and MDCT of Phantom 6 with permanent dentition

	Skull			CT		
	mean	SD	σi	mean	SD	σi
Upper W3	40.3	0.0	0.1	40.3	0.1	0.2
W6	57.9	0.1	0.1	57.7	0.1	0.2
Lower W3	31.7	0.1	0.1	31.5	0.3	0.3
W6	54.6	0.0	0.1	54.3	0.1	0.2

SD ; standard deviation, σi ; intraobserver errors

Table 8. Average of dental arch width in Skulls and MDCTs of primary and mixed dentition

	Skulls		CT		
	mean	SD	mean	SD	*t*-test
Upper Wc	33.9	3.7	34.3	4.0	0.9
WE	49.3	5.8	49.6	5.9	1.0
Lower Wc	27.4	2.6	27.7	3.0	0.9
WE	48.4	5.5	48.8	5.4	0.9

$p<0.05$ SD ; standard deviation

Table 9. Average of dental arch width in Skulls and MDCTs of permanent dentition

	Skulls		CT		
	mean	SD	mean	SD	*t*-test
Upper W3	39.3	1.5	39.4	1.3	0.9
W6	58.0	0.1	58.2	0.4	0.4
Lower W3	30.3	1.0	30.1	1.0	0.9
W6	52.9	1.6	53.0	1.6	1.0

$p<0.05$ SD ; standard deviation

width in phantoms and MDCT images were very similar. Table 5 shows the average mesiodistal diameter measurements of primary teeth and permanent teeth of the six phantoms. The differences of the mean mesiodistal diameter in upper and lower primary and permanent teeth between phantoms and MDCT images were less than 0.3 mm. Comparison of dental arch width on skull and MDCT images of Phantom 1 are shown in Table 6. Table 7 shows the mean dental arch width on phantom and MDCT images of Phantom 6. The average differences of the measurement of WC and WE in primary and mixed dentitions were within 0.4 mm (Table 8), and W3 and W6 on the six phantoms and MDCT images were less than 0.2 mm (Table 9). No significant differences were noted between them.

Discussion

In pediatric dentistry, determination of the physiological age and dental characteristics of child patients is essential to predict adult occlusion and proper dental treatment. Minor anomalies mostly occur in the craniofacial and oral regions. CT images are employed for diagnosis of some syndromes with mental retardation. Craniosynostosis is seen frequently in Apert, Crouzon and carpenter syndromes, delayed closure of fontanels is frequently seen in cleidocranial dysostosis and Down, Hallermann-Strief and Russell-Silver syndromes, maxillary hypoplasia with narrow and high arched palate are seen frequently in Crouzon, Marfan and Sotos syndromes, prognathism is seen frequently in Angelman, Gorlin and Sotos syndromes, micrognathia is seen frequently in Pierre Robin sequence and de Lange and Treacher-Collins syndromes, anodontia is seen frequently in ectodermal dysplasia and Ectrodactyly-ectodermal dysplasia-clefting syndrome (EEC), late eruption of teeth is seen frequently in cleidocranial dysostosis, de Lange syndromes and X-linked hypophosphatemic rickets, and microdontia is seen frequently in Down syndrome and ectodermal dysplasia. CT images are able to reveal the above anomalies in some syndromes with mental retardation (4).

In this study, the physiological age based on the development of permanent teeth was defined by the stages of Nolla (1), who discussed the development of permanent teeth at each physical age using a set of